DOI: 10.1002/ejic.200700146

The Thermal Decomposition of Three Magnetic Acetates at Their Autogenic Pressure Yields Different Products. Why?

Swati V. Pol,[a] Vilas G. Pol,[a] Israel Felner,[b] and Aharon Gedanken*[a]

Keywords: Decomposition / Acetates / Magnetic properties / Core-shell nanostructures

We report on the one-stage, reproducible, solvent-free, competent and straightforward approach for the synthesis of fullerene-like Ni@C, Co@C, and Fe_3O_4@C core-shell nanostructures that can be scaled up. The single precursor reactions of low cost acetates of Fe, Co and Ni are separately conducted at a relatively low temperature (700 °C) in a closed Swagelok reactor, as compared to other methods for the formation of graphitic layers. It is worth mentioning that although identical reaction parameters are employed, using the three acetate precursors, the graphitic carbon is coated on nanosized metallic Ni and Co cores, while Fe tends to form Fe_3O_4, maintaining the same core-shell morphology. The systematic morphological, compositional, structural characterization and the room temperature magnetic susceptibility measurements of the as-made particles are carried out on a vibrating sample magnetometer. The plausible mechanism is based on the comparison between the dissociation products of three acetate precursors, their obtained experimental data, and calculations on the enthalpy and free energy changes.

Introduction

The studies of magnetic nanoparticles and nanostructures combine a broad range of synthetic and investigative techniques from physics, chemistry, and materials science. Ultra fine magnetic particles have been the subject of intense scientific research in recent years with respect to their novel properties and commercially-potential valuable applications.[1] The application of the encapsulated magnetic nanomaterials ranges from magnetic inks, magnetic recording media, toners for xerography, and ferrofluids for biomedical applications, such as contrast agents in magnetic resonance imaging.[2] Single- and multi-walled carbon nanotubes filled with ferromagnetic materials (Fe, Co, Ni) showed significant potential in data storage.[3] The ferromagnetic nanosized Fe, Ni, or Co coated with carbon constitute a group of especially interesting magnetic nanomaterials. This is because of their fascinating magnetic properties, and the carbon coating that protects the magnetic nanoparticles against environmental degradation.[3] The discovery of fullerenes and carbon-coated materials accelerated extensive investigation on nanoparticles, carbon-coated nanomaterials, and a wide range of carbon-based materials.[4] Some of the standard problems encountered in the synthesis of nanoparticles are those of good control of composition, particle size and morphology, a narrow monodisperse size distribution, and stabilization against oxidation in the case of reactive metals.

Various synthetic methods of magnetic nanoparticles have been reported in recent times, e.g., wet chemical processes,[5–6] inert gas condensation,[7] ultra-rapid quenching and vacuum-based deposition.[8] Carbon nanotubes and filled carbon nanostructures such as onions, wires, and rods, have been prepared by the pyrolysis of metallocene.[9–10] Using Ni(acac) and Cu(acac) as catalyst precursors, carbon nanotubes and onions from carbon monoxide were produced previously.[11] An arc-discharge process[12] was employed for the preparation of ferromagnetic carbon-coated Fe, Co, and Ni nanoparticles. The major problem with the synthesis of graphite-encapsulated nanocrystals by using the standard arc method has been the production of large amounts of unwanted carbonaceous debris.[13] This causes the reduction of particle-exchange coupling, which is an important issue in the ongoing attempt to synthesize high density magnetic recording media.[14a] Vivekchand et al. recently developed a new method for the preparation of metal nanowires by the nebulized spray pyrolysis of precursors.[14b] The arc evaporation method is also successfully demonstrated for the encapsulation of ferromagnetic metals (iron, cobalt, and nickel) nanoparticles in graphitic carbon.[14c] Chemical vapor synthesis (CVS) is becoming increasingly important because of its potential for producing nanomaterials in a controlled and scalable way with a low degree of agglomeration.[15] Each technique has its own advantages and disadvantages. However, most of the techniques require a high energy input and are not suitable for

---

[a] Department of Chemistry and Kanbar Laboratory for Nanomaterials at the Bar-Ilan University Center for Advanced Materials and Nanotechnology, Bar-Ilan University,
Ramat-Gan, 52900, Israel
E-mail: gedanken@mail.biu.ac.il
[b] Rakah Institute of Physics, Hebrew University,
Jerusalem, 91904, Israel

mass production because of the low yield and the complicated process control. The research community is seeking methods for producing carbon nanomaterials with specific properties and on an industrial scale. Thus, further experimental research on their synthesis is needed.

Herein, we report on a one-stage, reproducible, solvent-free, competent, and straightforward approach for the synthesis of fullerene-like Ni@C, Co@C, and Fe_3O_4@C core-shell nanostructures that can be scaled up. The single precursor reactions of low-cost acetates of Fe, Co and Ni are conducted separately at a relatively low temperature (700 °C) in a closed Swagelok reactor, as compared to other methods for the formation of graphitic layers. It is worth mentioning that although identical reaction parameters are employed, using the three acetate precursors, graphitic carbon-coated nanosize metals are obtained for Ni and Co, while Fe tends to form Fe_3O_4, maintaining the same core-shell morphology. Early results on a similar reaction of $Ni(AcAc)_2$ have been reported.[16] This publication extends this report and also includes a comparison between Fe^{II}, Ni^{II}, and Co^{II} acetates, which yield different products. This manuscript also attempts to account for and explain the formation of different products. The systematic morphological, compositional, structural characterization and room temperature magnetic susceptibility measurements of the as-made particles are measured by using a vibrating sample magnetometer. The suggested mechanism is supported by the obtained experimental data and calculations on enthalpy, as well as free energy changes.

Results and Discussion

1. C, H, N, S, and O Analysis, X-ray Diffraction, Mössbauer, and BET Surface Area Measurements

Here we present and compare the results related to the three metal acetates that produce core/shell structures of metal/metal oxide surrounded by carbon. The carbon and hydrogen content in the product/carbonaceous material is determined by elemental analysis measurements (Table 1). The calculated element percentages of carbon in Ni, Co and Fe acetates are 27.2, 27.1, and 27.6%, while the element percentages of hydrogen are 3.4, 3.4, and 3.5%, respectively. The measured percentage of carbon in Ni@C, Co@C, and Fe_3O_4@C products are 11.78, 15.25, and 22.3 wt.-%, while the percentages of hydrogen are 0.18, 0.1, and 0.12%, respectively. The calculated oxygen percentage for Ni, Co, and Fe acetates is almost the same (ca. 36 wt.-%). The measured oxygen percentages are 0.2, 0.3, and 21.43 wt.-% for Ni@C, Co@C, and Fe_3O_4@C products, respectively. The calculated weight of metal Ni, Co, and Fe is 332 mg, 333 mg, and 321 mg in 1 g of nickel(II) acetate, cobalt(II) acetate, and iron(II) acetate precursors, while 337 mg, 339 mg, and 315 mg account for the 382 mg, 400 mg, and 560 mg of the Ni@C, Co@C, and Fe_3O_4@C products, respectively. It is obvious that the products show less carbon than the reactants, while the percent of hydrogen is almost negligible. This means that some of the carbon is bonded to the hydrogen in the form of hydrocarbons and/or to oxygen to form carbon oxides. Furthermore, the reduction in the transition metal is observed in both Ni@C and Co@C. This reduction might have occurred due to carbon monoxide. Jesus et al. reported on the thermal decomposition[17] process of the nickel acetate precursor under inert atmosphere. Our obtained coupled TGA-Mass spectroscopy analysis data for Ni acetate salt are in agreement with this. The TGA spectra of all the three acetates are shown in Figure 1.

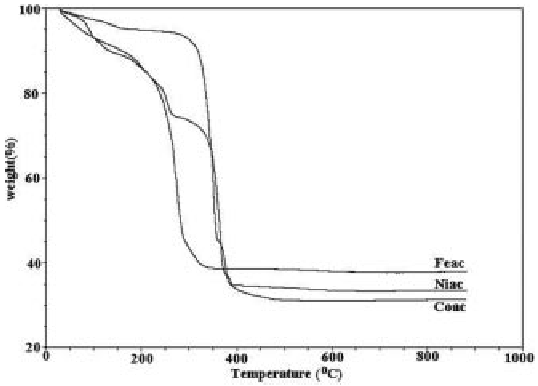

Figure 1. The TGA curve of Fe, Co, and Ni acetates.

The complete decomposition of all the acetates is observed at about 400 °C. The higher weight loss is observed for Ni and Co acetates (68%), while early (ca. 300 °C) and less weight loss (60%) accounts for Fe acetate. The residual weight of about 32% corresponds to the metallic Ni and Co for the related acetates, while the 40% for Fe acetate corresponds to FeO. The gaseous content of the dissociation products of these acetates at 350 °C is monitored by an MS. The gases detected by the instrument are acetone, CH_3COCH_3 ($m/z = 58$), acetic acid, CH_3COOH (60), CO_2 (44), CO (28), CH_4 (16), C_2H_6 (30), and C_2H_2 (26).

Conducting the RAPET reaction of all three acetates at 650 °C does not lead to any crystalline products, and only amorphous products are obtained, based on XRD mea-

Table 1. The obtained products, % yield, morphology, crystal structure, percent of carbon, hydrogen and oxygen and BET surface area are illustrated.

Sample name	% Yield	XRD	Morphology (TEM)	wt.-% C	wt.-% H	wt.-% O	BET Surface area m^2/g
Ni@C	38.2	Ni	core-shell	11.78	0.18	0.2	1
Co@C	40	Co	core-shell	15.25	0.10	0.3	3
Fe_3O_4@C	56	Fe_3O_4	core-shell	22.3	0.12	21.43	2

surements. The first crystalline products for the RAPET of the acetates appear at 700 °C. The RAPET of Ni and Co acetates in a closed cell at 700 °C yields 38.2% and 40% of products containing metallic Ni and Co, respectively coated with carbon. The dissociation of Fe acetate in a closed RAPET system confirms the weight loss of 44%, keeping about 56% of a solid product consisting of Fe_3O_4 and carbon. The rest of the weight loss is due to the formation of hydrocarbons and carbon oxides. In the case of the RAPET of Fe acetate, the reactant possesses a +2 oxidation state, while the product has a 2.66 oxidation state. This means that unlike Co and Ni ions, which undergo a reduction to the corresponding metals, the Fe^{+2} is partially oxidized to Fe_3O_4 before being coated by carbon. Since the particles are densely coated with graphitic carbon, the oxidation of the product due to handling under air atmosphere is impossible. It is noticeable that the Fe is more facile to oxidation than Ni and Co. The measured surface areas for the Ni@C, Co@C and Fe_3O_4@C products are 1, 3, and 2 m^2/g, respectively.

The XRD pattern of the as-prepared Ni@C sample is presented in Figure 2 (top). The diffraction peaks, observed at $2\theta = 44.49$, 51.85, and 76.38, are assigned as (111), (200), and (220) reflection lines of the face-centered cubic phase of Ni (space group: *Fm-3m*). These values are in good agreement with the diffraction peaks, peak intensities and cell parameters of crystalline Ni (PDF No. 87-712). The diffraction patterns of the as-prepared Co@C sample (middle) can be indexed to fcc (space group: *Fm-3m*) Co, and matches well with PDF No. 89-4307. The diffraction peaks observed at $2\theta = 44.22$, 51. 35, and 75.86 are assigned as (111), (200), and (220) reflection lines. The XRD pattern of the as-prepared Fe_3O_4@C sample is presented at the bottom of Figure 2. The major diffraction peaks are observed at $2\theta = 30.10$, 35.45, 37.08, 43.08, 53.45, 56.98, 62.57, and 74.02 and are assigned as (220), (311), (222), (400), (422), (511), (440) and (533) reflection lines. These values are in good agreement with the diffraction peaks, peak intensities and cell parameters of crystalline Fe_3O_4 (PDF No. 65-3107). However, since the XRD of γ-Fe_2O_3 is very similar to that of magnetite, we also used Mössbauer spectroscopy to further substantiate our assignment. In none of the three cases is a carbide phase detected. The small diffraction peak at $2\theta = 26.6°$, assigned to graphitic carbon, is only detected for Co@C, and is suppressed in Ni and Fe_3O_4.

The Mössbauer spectra of Fe_3O_4 at 298 K are shown in Figure 3. The spectra show two hyperfine magnetic splits, which are clear evidence for the existence of Fe_3O_4 (magnetite). In the transmission spectrum, the hyperfine split arises due to a nuclear quadrupole interaction. This indicates that there is some departure from the cubic symmetry of the electric field due to the existence of an electric field gradient at the nucleus. It means that the ^{57}Fe excited level ($I = {}^3/_2$) has split, whereas the ground state ($I = {}^1/_2$) remains whole/intact. The difference in energy levels is only due to different electronic densities of the Fe atoms at the source, and the absorber. Fe_3O_4 can be written as $[(Fe^{3+})(Fe^{2+}Fe^{3+})]O_4$. The magnetic hyperfine fields of 455 and 487 kOe and the two isomer shift values, 0.67 and 0.37 mm/s, correspond to site A (Fe^{3+}) ions and to site B (Fe^{2+}, Fe^{3+}) ions, respectively. The high isomer shift for the B site is typical for Fe^{2+}. The resultant parameters are given in Table 2.

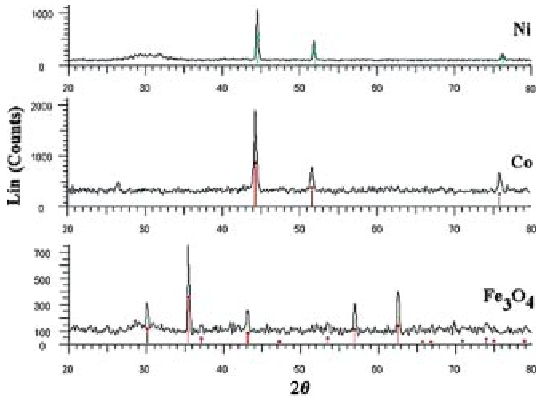

Figure 2. XRD patterns of as-prepared Ni@C (top), Co@C (middle), and Fe_3O_4@C (bottom) samples.

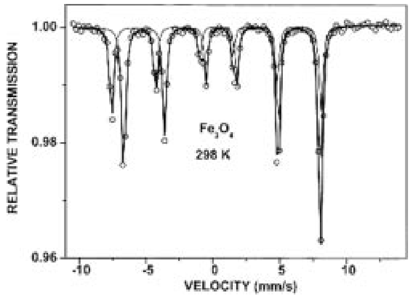

Figure 3. The Mössbauer spectrum of a Fe_3O_4@C sample at room temperature.

Table 2. The Mössbauer parameters of Fe_3O_4@C sample: isomeric shift (mm/s), quadrupole moment (mm/s) and effective field (kOe) for site A and site B.

	I.S. (mm/s)	eQ (mm/s)	H_{eff} (kOe)
Site A	0.67	0.028	455
Site B	0.37	–	487

The nature of the coated carbon for all of three samples is also studied by employing Raman spectroscopy and HR-TEM measurements.

2. TEM, SEM, EDS, Raman, and HR-TEM Measurements

The morphology of all the samples is studied by TEM measurements. The transmission electron micrograph of Ni@C core-shell structures is shown in part a of Figure 4. The thermal dissociation of Ni acetate favors the formation of the dark particles of Ni, which are coated with carbon layers. We assume that the thermal decomposition of $Ni(CH_3COO)_2$, leads to dissociation into carbon, hydrogen, oxygen and nickel atoms at 700 °C. The Ni atoms forms the Ni core. The particle diameters range from 20 nm to 160 nm. The high resolution image (Figure 4b) taken on a single particle revealed that the 25 nm dark core of Ni is encapsulated in 5–10 nm carbon layers. Using the SAEDS technique, the identification of the dark cores as Ni, Co and iron oxide, which are covered by carbon, is confirmed for all the three products of (Ni, Co, and Fe) acetates. The TEM image of the Co@C sample demonstrates (Figure 4c) that the particles, whose diameters range from 30 to 230 nm, are covered with in situ formed carbon layers after the dissociation of cobalt acetate. The central 110 nm diameter cobalt particle is uniformly surrounded by a 20 nm carbon layer (Figure 4d). Thus, a similar trend is observed for the thermal decomposition of $Co(CH_3COO)_2$ and $Ni(CH_3COO)_2$, resulting in a metallic core and a carbon shell structure. Part e of Figure 4 shows that the 5 to 20 nm particles of Fe_3O_4 are densely covered with carbon. The HR-TEM image (Figure 4f) of a 10 nm Fe_3O_4 particle is surrounded by a thick layer of carbon. The thermal dissociation of Fe acetate favors the formation of a Fe_3O_4 core, which is coated with carbon layers after the decomposition of $Fe(CH_3COO)_2$. This means that the produced carbon, hydrogen, oxygen and FeO facilitate the FeO to react with oxygen to form Fe_3O_4, thus hindering the reduction.

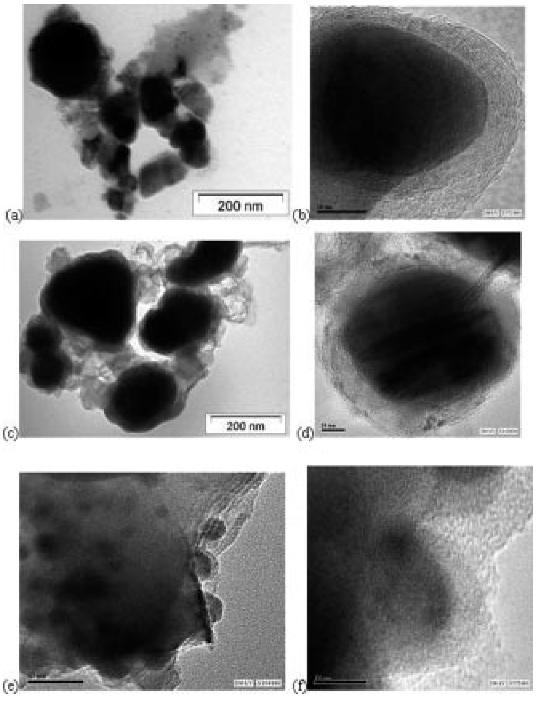

Figure 4. Transmission electron micrographs of (a) Ni@C sample, (b) single Ni@C particle at high resolution, (c) Co@C sample, (d) single Co@C particle at high resolution, (e) Fe_3O_4@C sample, and (f) single Fe_3O_4@C particle at high resolution.

The SEM image shown in Figure 5a indicates the spherical morphology of the Ni@C. The Ni-C particles have a tendency to form a few agglomerates, which are observed in addition to the individual particles. The aggregation is attributed to their magnetic nature. The diameters of the separated individual particles are in the range of 40–160 nm. The EDS of the Ni@C particles is presented in Figure 5b, and confirms the presence of Ni and C. No additional peak is detected, which verifies the purity of the Ni@C sample.

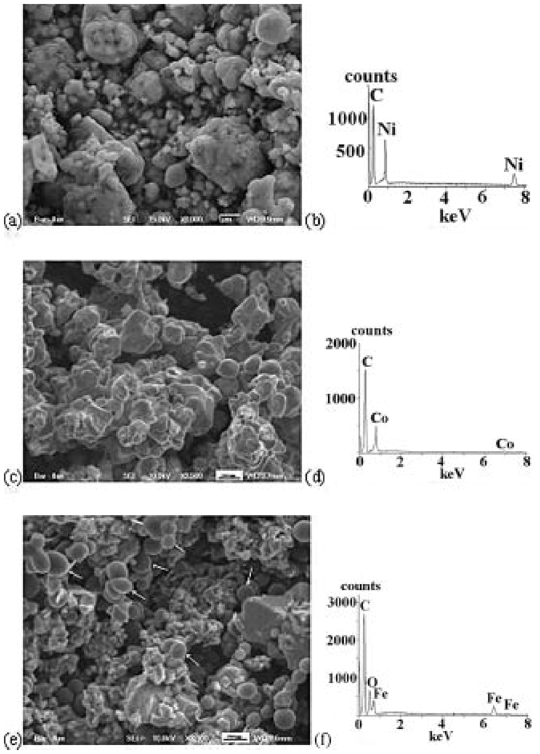

Figure 5. Scanning electron micrographs of (a) Ni@C sample, (b) EDS of Ni@C sample, (c) Co@C sample, (d) EDS of Co@C sample, (e) Fe_3O_4@C sample [arrow indicates egg-like carbon entities], and (f) EDS of Fe_3O_4@C sample.

The SEM image of the Co@C sample demonstrates (Figure 5c) that the particle diameter ranges from 50 to 200 nm. In addition, the obvious aggregating tendency of magnetic Co@C particles is observed. The EDS analysis of the Co@C sample (Figure 5d) detected only the presence of cobalt and carbon, without additional impurities. Negligible amounts of oxygen are detected in Ni@C and Co@C samples.

The Fe_3O_4@C sample possesses an oval shaped mixture of about 400 nm and aggregates of about 100 nm particles (Figure 5e). The SAEDS confirm that the oval shaped particles, indicated by an arrow, are composed solely of carbon, while the smaller particles are composed of Fe_3O_4 and carbon. The core-shell nature of Fe_3O_4 surrounded by C is substantiated by TEM measurements. The excess of carbon might have lead to the formation of egg-like carbon entities in the Fe_3O_4@C sample. The bulk EDS analysis of the Fe_3O_4@C sample is shown in part f of Figure 5, presented Fe, O, and carbon occurrence. The formation of Fe_3O_4 and carbon without additional impurities is confirmed by the EDS spectrum shown in Figure 5f.

The nature of the carbon shell is investigated by Raman spectroscopy. The Raman spectra (Figure 6) are the characteristics of disordered graphitic carbon with nanosized graphitic crystals. The first D peak, located at ca. 1330 cm^{-1}, originates from the in-plane lattice vibrations. The second G peak is located at ca. 1595 cm^{-1}, and only occurs when small, crystal-size graphitic particles are present.[18] The D band is associated with graphitic edge-planes and defects in the graphitic lattice. The relative intensity of the D and G bands is generally used to estimate the size of graphitic clusters in the hexagonal plane, *La*. Although all the samples are prepared at 700 °C, the intensity of graphitic carbon is much higher than the disordered carbon for the Ni@C sample. Almost the same intensity is observed for the Co@C and Fe_3O_4@C samples. The results indicate that Ni is the best catalyst for the preparation of high order graphitic planes. This is also manifested in the relatively low temperature that the graphitic layers reach.

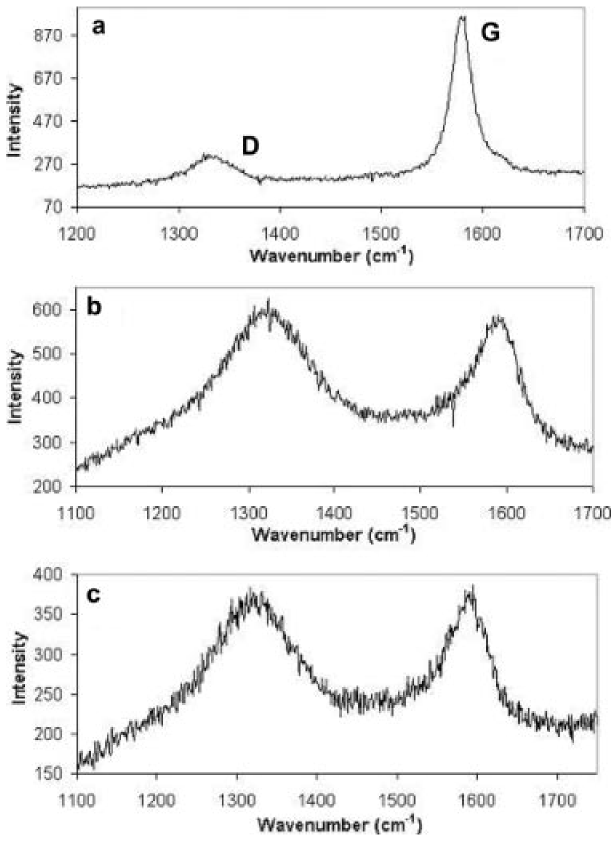

Figure 6. Raman spectra of a) Ni@C, b) Co@C, and c) Fe_3O_4@C samples.

In order to understand the graphitization of formed carbon layers around the cores, HR-TEM measurements of the carbon-shells are carried out for the Ni@C, Co@C, and Fe_3O_4@C samples. The measured interlayer spacings between these graphitic planes are 0.345, 0.337, and 0.341 nm for Ni@C (Figure 7a), Co@C (Figure 7b), and Fe_3O_4@C (Figure 7c) samples, respectively, which are very close to that of the graphitic layers. It should be noted that the graphitic ordering is much better in Ni than in the Co and Fe_3O_4.

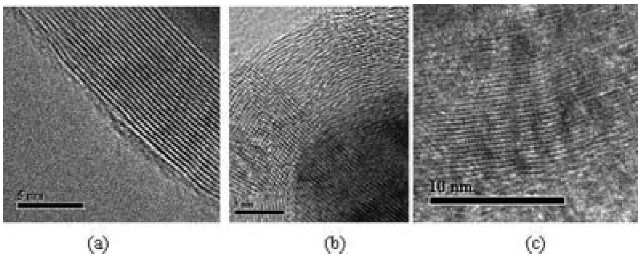

Figure 7. HR-TEM images of a) carbon layer coated on the Ni core, b) carbon coated on the Co core, and c) carbon layer on the surface of Fe_3O_4 core.

To summarize, the few points that need further clarification and discussion on the results reported for the decomposition of all three acetates (Co, Ni, and Fe) are: 1) The cores of Co, Ni, and iron oxide are surrounded by graphitic carbon (interlayer spacing ≈ 0.34 nm). 2) A wide particle size distribution is observed. 3) The thickness of the carbon coating around the cores is proportional to the percentage of carbon present in the product (see Table 1). 4) Although the graphitic carbon encapsulates the cores, nanosize Ni and Co are obtained in metallic form, while Fe tends to form Fe_3O_4 (confirmed by XRD, EDS, and SAEDS), maintaining the core-shell morphology. The three-dimensionality of the onion-like structures of Ni@C, Co@C, and Fe_3O_4@C products is confirmed by tilting the TEM grid during HR-TEM measurements, when the pictures remained unchanged.

3. Magnetic Properties

A room temperature magnetic susceptibility measurement of Ni@C, Co@C, and Fe_3O_4@C samples is conducted by employing a vibrating sample magnetometer. A small amount of material, ca. 20 mg, is inserted into a plastic capsule. Cotton wool is placed on the top of the sample and the capsule is sealed. This prevents the particles from any movement caused by the vibration of a VSM sample holder rod, or by a variation in the applied magnetic field during measurements. The magnetization vs. magnetic field curves are measured for all the samples (Figure 8a–c) in the range of –15800 to 16000 Oe.

The Ni@C sample exhibits typical hysteresis with a saturation magnetization of 21.7 emu/g (Figure 8a). Taking into account the fact that the sample contains 11.78% carbon and the remaining 88.22% Ni, this yields a value of 24.6 emu/g for 100% Ni. A 151 Oe coercive field is obtained for the Ni@C sample. The Co@C sample shows a saturation magnetization of 21.87 emu/g (Figure 8b). When considering that the sample contains 84.75% of Co, this gives a value of 25.81 emu/g for 100% Co. This sample shows the coercivity of 97 Oe with a remanent magnetization of 2.6 emu/g. Figure 8c shows the magnetization curve of the Fe_3O_4@C sample. Unlike the ferromagnetic behavior detected for Ni@C and the Co@C, the characteristic behavior of superparamagnetic particles is detected for Fe_3O_4@C. The magnetization curve does not show hysteresis and does

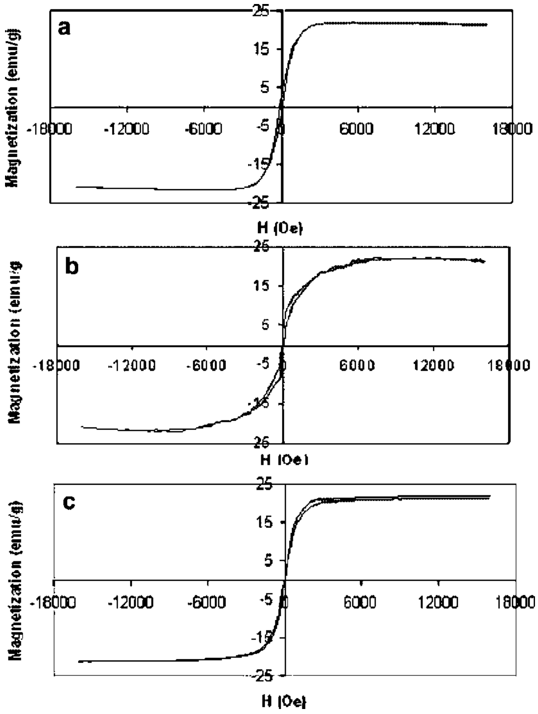

Figure 8. Magnetization vs. magnetic field curves for a) Ni@C, b) Co@C, and c) Fe_3O_4@C samples.

not saturate (a small increase in magnetization is measured between 12–16 kOe), even at 16 kOe. This is due to the Fe_3O_4 core, which is comprised of small 5–20 nm crystallites (shown in the TEM measurements). The magnetization of ferromagnetic materials is very sensitive to the microstructure of a sample. If a specimen consists of small particles, its total magnetization decreases with decreasing particle size due to the increased dispersion in the exchange integral,[19] finally reaching the superparamagnetic state, when each particle acts as a big 'spin' with suppressed exchange interaction between the particles, which is more hindered because of the presence of the carbon shell. Nanomagnetic particles are expected to exhibit reduced magnetization due to the large percentage of surface spins with disordered magnetization orientation.[20] In fact, the magnetization is smaller than the bare particles, indicating that there is no magnetic proximity effect between the magnetic (Ni, Co, or Fe_3O_4) particles and carbon, which is consistent with recent experiments.[21]

The main question remaining now is why are Ni and Co obtained in the metallic form, while Fe tends to form Fe_3O_4, maintaining a carbon shell in all three cases. The thermal decomposition of $Ni(CH_3COO)_2$ at 350 °C[17] leads to dissociation into nickel oxide and oxygenates like acetone and acetic acid, as perceived by TGA coupled with MS. It is worth mentioning that both, Jesus et al.[17] and our own TGA + MS results show that CO is one of the intermediates in the decomposition of the Ni acetate. We attribute the reduction of nickel oxide to carbon monoxide. The product of the reduction is the Ni atom, forming the Ni core, while the oxygenate molecule decomposes to hydrocarbon, and further to carbon. In our previous RAPET reactions of various organic or organometallic materials, we observed the appearance of carbon above 550 °C.[22–24]

The decomposition of $Co(ac)_2$ and $Ni(ac)_2$ results in a metallic core and carbon shell structures, while the thermal dissociation of Fe acetate favors the formation of a Fe_3O_4 core, which is coated with graphitic and disordered carbon layers. It should be noted that the only source of oxygen is the acetate ion, and its quantity in all three acetates is almost the same (36 wt.-%).

Based on the obtained MS data, we propose the dissociation of acetates as follows:

$$M(CH_3COO)_2 \rightarrow MCO_3 + CH_3COCH_3 \qquad (1)$$

$$MCO_3 \rightarrow MO + CO_2 \qquad (2)$$

$$CH_3COCH_3 \rightarrow CO + C_2H_6 \qquad (3)$$

$$MO + CO \rightarrow M + CO_2 \qquad (4)$$

where M = Ni, Co, Fe.

The formation of the first oxygenated product, acetone, occurs by Equation (1). The metal carbonate,[17,25] which is a short-lived intermediate, immediately decarboxylates to give a metal oxide at 350 °C. This metal oxide, in the case of Ni and Co acetates, gets reduced by carbon monoxide, while the Fe atoms prefer to stay as FeO. It further is oxidized to form Fe_3O_4 and then coated by carbon to form the core-shell structure during solidification. This can be explained by the reduction potential values of Ni, Co, and Fe. The well-known standard reduction potentials[26] at 25 °C for Ni, Co and Fe are –0.25, –0.27, and –0.44 V, respectively, for the metal–metal ion equilibrium. These numbers indicate that iron is less favorably reduced than cobalt and nickel.

Thus, all three acetates decompose into their corresponding oxides, which further get reduced by carbon monoxide to a metallic form. The values for the enthalpy change, ΔH^0, and free energy change, ΔG^0, are calculated to form the respective metals from the corresponding oxide[27] in the presence of carbon monoxide at 700 K. Since the cases of Ni and Co are similar, the values are calculated for the representative Co@C case and, for simplicity, are compared with the case of Fe_3O_4@C.

$FeO(s) + CO(s) \rightarrow Fe_{(s)} + CO_2(g)$
$\Delta H^0 = -14.7$ kJ/mol at 700 K
$\Delta G^0 = +3.55$ kJ/mol at 700 K
$CoO(s) + CO(s) \rightarrow Co(s) + CO_2(g)$
$\Delta H^0 = -49.89$ kJ/mol at 700 K
$\Delta G^0 = -37.61$ kJ/mol at 700 K

The positive value obtained for the ΔG^0 of formation of Fe from Fe^{II} acetate, unlike Ni and Co, indicates that thermodynamically, the reduction to the metallic state is not favorable. Therefore, the alternative is its partial oxidation and the kinetically-controlled coating by the carbon surrounding it, forming the Fe_3O_4@C. On the other hand, the ΔG^0 value is negative for the formation of metallic cobalt and Ni, and we assume that the reaction is also fast. Thus the core of metallic Co or Ni is formed in this way in Co@C and Ni@C particles.

Conclusions

In summary, using low cost, transition metal acetate precursors and employing identical reaction parameters, graphitic carbon-coated nanosize Ni, Co are obtained in the metallic form. Metallic Fe is not obtained, and instead it forms Fe_3O_4, maintaining the core-shell morphology. A broad particle size distribution is observed. Graphite-encapsulated Ni, Co, and Fe_3O_4 fullerene-like core-shell nanostructures could be obtained at a relatively low temperature (700 °C) in a closed Swagelok reactor, as compared to other methods for the formation of graphitic layers. The one-stage, reproducible, solvent-free, competent and straightforward approach for the synthesis of Ni@C, Co@C, and Fe_3O_4@C core-shell nanostructures can be scaled up.

Experimental Section

Synthesis of Fullerene-like Ni@C, Co@C and Fe_3O_4@C Core-Shell Nanostructures: Acetates of Fe^{II} (Aldrich), Co^{II} (Aldrich) and Ni^{II} (Alfa Aesar), were purchased with > 99% purity and used as received. In the fabrication of Ni@C, Co@C, and Fe_3O_4@C core-shell nanostructures, 1 g of the acetate of Ni, Co and Fe are introduced separately into a 3 mL stainless steel reactor at room temperature in a nitrogen-filled glove box. The filled Swagelok reactors are closed tightly with the other plug.[22] The temperature of the tube furnace is raised to 700 °C at a rate of 10 °C/min, and the temperature is maintained at 700 °C for 3 h. The Swagelok-reactors heated at 700 °C are gradually cooled (ca. 6 h) to room temperature and opened. A black powders of Ni@C (0.382 g), Co@C (0.400 g) and Fe_3O_4@C (0.560 g) is obtained. The obtained products, their morphology, crystal structure, carbon percent are shown in Table 1. Earlier, such a one-stage, efficient, and the simplest economic RAPET (Reactions under Autogenic Pressure at Elevated Temperature) technique was employed for the fabrication of various interesting nanostructures.[22–24]

Characterization: Various analytical techniques are used to identify and characterize the as-prepared RAPET products of the Ni, Co and Fe acetate reactions. To understand the purity of the crystal structure (the interatomic distance, and angle) of the as-prepared products, the X-ray diffraction patterns are measured with a Bruker AXS D* Advance Powder X-ray diffractometer [$\lambda(\text{Cu-}K_a)$ = 1.5418 Å]. Since all the acetate contains C, H, and O, in addition to metal, C, H, N, S and O analyses are carried out for the as-prepared products on an Eager 200 C,H,N,S analyzer and an EA1110, oxygen analyzer, respectively. The morphology, grain size, and chemical composition in a selected area are measured for the fullerene-like Ni@C, Co@C, and Fe_3O_4@C core-shell nanostructures by employing transmission electron microscopy (TEM) (JEM-1200EX) and high-resolution transmission electron microscopy (HRTEM) (JOEL 2010), working at acceleration voltages of 80 kV and 200 kV, respectively. The morphology and energy dispersive X-ray analysis (EDX) of the materials are investigated by high resolution scanning electron microscopy (HR-SEM, JSM, 7000 F). The Mössbauer spectroscopy (MS) studies are carried out at room temp. using a conventional constant acceleration spectrometer. The ^{57}Fe MS are measured with a 50 mCi ^{57}Co:Rh source and the spectra were least square fitted with two sub spectra. The isomer shift (IS) values are relative to Fe metal at 300 K. A Micromeritics (Gemini 2375) surface area analyzer is used to measure the surface area of the samples. An Olympus BX41 (Jobin–Yvon–Horiba) Raman spectrometer is employed, using the 514.5 nm line of an Ar ion laser as the excitation source to analyze the nature of the carbon present in the samples. A vibrating sample magnetometer (VSM-Oxford-3001) is used for the magnetic susceptibility measurements for Ni@C, Co@C, and Fe_3O_4@C samples at room temperature.

[1] W. Krätschmer, L. D. Lamb, K. Fostiropoulos, D. R. Huffman, *Nature* **1990**, *347*, 354.

[2] T. Hayashi, S. Hirono, M. Tomita, S. Umemura, *Nature* **1996**, *381*, 772.

[3] A. Leonhardt, M. Ritschel, R. Kozhuharova, A. Graff, T. Muhl, R. Huhle, I. Monch, D. Elefant, C. M. Schneider, *Diamond Relat. Mater.* **2003**, *12*, 790–793.

[4] H. W. Kroto, J. R. Keath, S. C. O'Brien, R. F. Curl, R. E. Smalley, *Nature* **1985**, *318*, 162–165.

[5] L. Guo, Q. J. Huang, X. Y. Li, S. H. Yang, *Phys. Chem. Chem. Phys.* **2001**, *3*, 1661.

[6] T. Hyeon, *Chem. Commun.* **2003**, *8*, 927.

[7] S. Gangopadhyay, G. C. Hadjipanayis, B. Dale, C. M. Sorensen, K. J. Klabunde, V. Papaefthymiou, A. Kostikas, *Phys. Rev. B* **1992**, *45*, 9778.

[8] R. Sen, A. Govindaraj, C. N. R. Rao, *Chem. Phys. Lett.* **1997**, *267*, 276.

[9] C. N. R. Rao, R. Sen, B. C. Satishkumar, A. Govindaraj, *Chem. Commun.* **1998**, 1525.

[10] B. K. Pradhan, T. Kyotani, A. Tomita, *Chem. Commun.* **1999**, 1317.

[11] A. G. Nasibulin, A. Moisala, D. P. Brown, E. I. Kauppinen, *Carbon* **2003**, *41*, 2711–2724.

[12] J. Jiao, S. Seraphin, X. Wang, J. C. Withers, *J. Appl. Phys.* **1996**, *1*, 80.

[13] J. J. Host, J. A. Block, K. Parvin, V. P. Dravid, J. L. Alpers, T. Sezen, R. LaDuca, *J. Appl. Phys.* **1998**, *2*, 83.

[14] a) T. Yogi, T. Nguyen, *IEEE Trans. Magn.* **1993**, *29*, 307; b) S. R. C. Vivekchand, G. Gundiah, A. Govindaraj, C. N. R. Rao, *Adv. Mater.* **2004**, *16*, 1842; c) S. R. Sen, R. Subbanna, G. N. Kannan, C. N. R. Rao, *Chem. Phys. Lett.* **1995**, *31*, 308.

[15] S. Klein, M. Winterer, H. Hahn, *Chem. Vap. Deposition* **1998**, *4*, 143.

[16] S. V. Pol, V. G. Pol, A. Frydman, G. N. Churilov, A. Gedanken, *J. Phys. Chem. B* **2005**, *109*, 9495.

[17] J. C. De Jesus, I. Gonzalez, A. Quevedo, T. Puerta, *J. Mol. Catal. A* **2005**, *228*, 283.

[18] Y. Lifshitz, *Diamond Relat. Mater.* **1999**, *8*, 1659.

[19] S. R. Elliott, *Physics of Amorphous Materials*, Longman, London, New York, **1984**, p. 350.

[20] H. R. Kodoma, A. E. Berkovitz, E. J. Mcniff Jr, S. Foner, *Phys. Rev. Lett.* **1996**, *77*, 394.

[21] R. Hohne, M. Ziese, P. Esquinazi, *Carbon* **2004**, *42*, 3109.

[22] S. V. Pol, V. G. Pol, A. Gedanken, *Chem. Eur. J.* **2004**, *10*, 4467–4473.

[23] a) V. G. Pol, S. V. Pol, A. Gedanken, *J. Phys. Chem. B* **2005**, *109*, 6121; b) S. V. Pol, V. G. Pol, V. G. Kessler, G. A. Seisenbaeva, M. Sung, S. Asai, A. Gedanken, *J. Phys. Chem. B* **2004**, *108*, 6322; c) V. G. Pol, S. V. Pol, B. Markovsky, J. M. Calderon-Moreno, A. Gedanken, *Chem. Mater.* **2006**, *18*, 1512; d) S. V. Pol, V. G. Pol, A. Gedanken, *Adv. Mater.* **2006**, *18*, 2023.

[24] a) S. V. Pol, V. G. Pol, G. Seisenbaeva, V. G. Kessler, A. Gedanken, *Chem. Mater.* **2004**, *16*, 1793; b) V. G. Pol, S. V. Pol, A. Gedanken, *Chem. Mater.* **2005**, *17*, 1797; c) S. V. Pol, V. G. Pol, V. G. Kessler, G. A. Seisenbaeva, L. A. Solovyov, A. Gedanken, *Inorg. Chem.* **2005**, *44*, 9938; d) V. G. Pol, S. V. Pol, A. Gedanken, S. H. Lim, Z. Zhong, J. Lin, *J. Phys. Chem. B* **2006**, *110*, 11237.

[25] G. A. M. Hussein, A. K. H. Nohman, K. A. M. Attiya, *J. Therm. Anal.* **1994**, *42*, 1155.

[26] A. J. Bard, R. Parsons, J. Jordan, *Standard Potentials in Aqueous Solutions*, IUPAC, Marcel Dekker, New York, USA, **1985**.
[27] M. W. Chase Jr, C. A. Davies, J. R. Downey Jr, D. J. Frurip, R. A. McDonald, A. N. Syverud, *JANAF Thermochemical Tables*, 3rd ed., part I–III, ACS and Chemical Institute of Physics for the National Bureau of Standards, J. Phys. and Chem. Reference data, 14, **1985**, supplement no. 1.

Received: December 8, 2006